Biophysical Journal Volume 68 March 1995 1110–1119

Photophysics of the Fluorescent Ca^{2+} Indicator Fura-2

Viviane Van den Bergh,* Noël Boens,* Frans C. De Schryver,* Marcel Ameloot,‡ Paul Steels,‡ Jacques Gallay,§ Michel Vincent,§ and Andrzej Kowalczyk¶

*Department of Chemistry, Katholieke Universiteit Leuven, B-3001 Heverlee, Belgium; ‡Limburgs Universitair Centrum, B-3590 Diepenbeek, Belgium; Laboratoire pour l'Utilisation du Rayonnement Electromagnétique, Centre Universitaire Paris-Sud, 91405 Orsay, France; and Nicholas Copernicus University, 87-100 Torun, Poland

ABSTRACT The photophysics of the complex forming reaction of Ca^{2+} and Fura-2 are investigated using steady-state and time-resolved fluorescence measurements. The fluorescence decay traces were analyzed with global compartmental analysis yielding the following values for the rate constants at room temperature in aqueous solution with BAPTA as Ca^{2+} buffer: $k_{01} = 1.2 \times 10^9\ s^{-1}$, $k_{21} = 1.0 \times 10^{11}\ M^{-1}\ s^{-1}$, $k_{02} = 5.5 \times 10^8\ s^{-1}$, $k_{12} = 2.2 \times 10^7\ s^{-1}$, and with EGTA as Ca^{2+} buffer: $k_{01} = 1.4 \times 10^9\ s^{-1}$, $k_{21} = 5.0 \times 10^{10}\ M^{-1}\ s^{-1}$, $k_{02} = 5.5 \times 10^8\ s^{-1}$, $k_{12} = 3.2 \times 10^7\ s^{-1}$. k_{01} and k_{02} denote the respective deactivation rate constants of the Ca^{2+} free and bound forms of Fura-2 in the excited state. k_{21} represents the second-order rate constant of binding of Ca^{2+} and Fura-2 in the excited state, whereas k_{12} is the first-order rate constant of dissociation of the excited Ca^{2+}:Fura-2 complex. The ionic strength of the solution was shown not to influence the recovered values of the rate constants. From the estimated values of k_{12} and k_{21}, the dissociation constant K_d^* in the excited state was calculated. It was found that in EGTA Ca^{2+} buffer pK_d^* (3.2) is smaller than pK_d (6.9) and that there is negligible interference of the excited-state reaction with the determination of K_d and $[Ca^{2+}]$ from fluorimetric titration curves. Hence, Fura-2 can be safely used as an Ca^{2+} indicator. From the obtained fluorescence decay parameters and the steady-state excitation spectra, the species-associated excitation spectra of the Ca^{2+} free and bound forms of Fura-2 were calculated at intermediate Ca^{2+} concentrations.

INTRODUCTION

The fluorescent indicator for Ca^{2+}, Fura-2, developed by R. Y. Tsien and associates was a significant step forward in the determination of intracellular Ca^{2+} concentrations (Grynkiewicz et al., 1985; Cobbold and Rink, 1987; Tsien, 1991). Fura-2 is now the most popular Ca^{2+} probe, particularly in measurements of Ca^{2+} in single cells (Iaizzo et al., 1989; Bush and Jones, 1990; Moore et al., 1990). In comparison with previously developed Ca^{2+} indicators, Fura-2 has a higher quantum yield of fluorescence and higher molar extinction coefficients. Therefore, a good signal-to-noise ratio can be obtained at low probe concentration resulting in less disturbance of biological systems. The ground-state dissociation constant, K_d, for the Ca^{2+}/Fura-2 complex is around 200 nM, a value close to levels of cytoplasmic Ca^{2+} concentrations in cells. Ca^{2+} binds to Fura-2 with a simple 1:1 stoichiometry and causes the fluorescence excitation spectrum to shift to lower wavelength. The fluorescence emission spectrum of Fura-2 is virtually insensitive to $[Ca^{2+}]$. The magnitude of the fluorescence signal depends on $[Ca^{2+}]$. The ratio of the fluorescence signals at dual excitation wavelengths is independent of the actual amount of indicator in the cell and can be used to determine intracellular Ca^{2+} concentrations (Grynkiewicz et al., 1985; Tsien et al., 1985). When the indicator concentration cannot be held constant in different samples due to photobleaching or leakage, the ratio method is the method of choice. The ratio of the fluorescence intensities at 340 and 380 nm as excitation wavelengths and 510 nm as emission wavelength are generally used to determine the intracellular $[Ca^{2+}]$ with Fura-2 as fluorescent indicator. From this ratio, the level of intracellular $[Ca^{2+}]$ can be estimated by comparison with calibration curves obtained in vitro or in vivo (Grynkiewicz et al., 1985; Cobbold and Rink, 1987; Tsien, 1991).

It is not generally acknowledged that the binding reaction of Ca^{2+} and Fura-2 in the excited state and the corresponding dissociation of the formed excited-state complex could severely distort the results derived from fluorescence measurements. The degree of interference of the excited-state reaction with the determination of K_d and $[Ca^{2+}]$ depends on the values of the four rate constants defining the excited-state reaction. These values can be assessed by the analysis of time-resolved fluorescence experiments. So far, only one study (Keating and Wenzel, 1991) has been published describing time-resolved fluorescence measurements of Fura-2. The obtained fluorescence decays were analyzed in terms of a biexponential decay law. However, this study did not provide any information about the rates of interconversion of the Ca^{2+} free and bound forms of Fura-2 in the excited state.

Time-resolved fluorimetry is an ideal technique to unravel the often complex kinetics of excited-state processes (O'Connor and Phillips, 1984; Boens, 1991). Fluorescence decay curves can be collected under various

Received for publication 21 April 1994 and in final form 12 October 1994.

Address reprint requests to Dr. Noel Boens, Department of Chemistry, Katholieke Universiteit Leuven, B-3001 Heverlee, Belgium. Tel.: 32-16-200656; Fax: 32-16-201215; E-mail: Noel@mds.chem.Kuleuven.ac.be.

A preliminary account of this research was presented at the SPIE meeting "Time-Resolved Laser Spectroscopy in Biochemistry IV" Los Angeles, California, 24–26 January 1994.

0006-3495/95/03/1110/10 $2.00

experimental conditions and with high accuracy allowing a detailed data analysis. All related experimental fluorescence decay traces can be analyzed simultaneously to enhance the capacity to distinguish between competing models and to obtain the most reliable parameter estimates. To benefit the most of the merits of this global analysis approach, one has to fit directly for the rate constants, the relative absorbances of the species in the ground state and the spectral emission weighting factors. This implementation has been called the global compartmental analysis and was presented in a series of articles from this laboratory (Ameloot et al., 1991, 1992; Van den Berg et al., 1992).

Before any new fluorescent molecule is proposed as a fluorescent indicator for biologically important ions or molecules, time-resolved fluorescence measurements should be performed to estimate values of the four rate constants defining the excited-state reaction. Using these values and the theory developed in this paper allows one to predict if the determination of the ground-state dissociation constant K_d from fluorimetric titration is undisturbed by the excited-state reaction. This general approach is exemplified here for Fura-2. Therefore, the photophysics of the reversible complex formation of Fura-2 and Ca^{2+} is studied in detail, using the global compartmental analysis approach. Application of the analytical expressions for the fluorescence signal in the absence and presence of an excited-state reaction indicates that the determination of K_d and/or $[Ca^{2+}]$ is not influenced by the excited-state complex formation and dissociation. Hence, Fura-2 can be safely used as a Ca^{2+} indicator.

THEORY

Kinetics

Consider a causal, linear, time-invariant, intermolecular system consisting of two distinct types of ground-state species and two corresponding excited-state species as is depicted in Scheme 1. Ground-state species 1 can reversibly react with M to form ground-state species 2. Excitation by light creates the excited-state species 1* and 2*, which can decay by fluorescence (F) and nonradiative (NR) processes (internal conversion (IC) and intersystem crossing (ISC)). The composite rate constants for these processes are denoted by k_{01} ($=k_{F1} + k_{NR1} = k_{F1} + k_{IC1} + k_{ISC1}$) and k_{02} ($=k_{F2} + k_{NR2} = k_{F2} + k_{IC2} + k_{ISC2}$). The second-order rate constant describing the transformation $1^* + M \rightarrow 2^*$ is represented by k_{21}. The first-order rate constant for the dissociation of 2* into 1* and M is denoted by k_{12}. In the case of Fura-2, species 1 represents the ground state of the free form of the indicator, species 2 the ground state of the complex between Ca^{2+} and Fura-2, and M denotes the Ca^{2+} ion. 1* and 2* are their corresponding excited-state species. If the system depicted in Scheme 1 is excited by a δ-pulse that does not significantly alter the concentrations of the ground-state species, the fluorescence δ-response function, $f(\lambda^{em}, \lambda^{ex}, t)$, at emission wavelength λ^{em} due to excitation at λ^{ex} is given by (Ameloot et al., 1991)

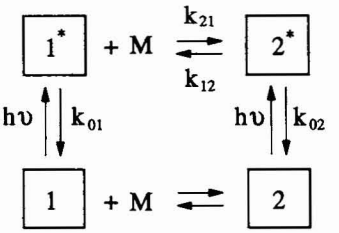

Scheme 1

$$f(\lambda^{em}, \lambda^{ex}, t) = \mathbf{c}(\lambda^{em})\mathbf{U}\exp(t\Gamma)\mathbf{U}^{-1}\mathbf{b}(\lambda^{ex}), \quad t \geq 0 \tag{1}$$

$\mathbf{U} = [\mathbf{U}_1, \mathbf{U}_2]$ is the matrix of the two eigenvectors of the compartmental matrix $\mathbf{A}$ (Eq. 2) and $\mathbf{U}^{-1}$ the inverse of $\mathbf{U}$. γ_1 and γ_2 are the eigenvalues of $\mathbf{A}$ corresponding to the eigenvectors $\mathbf{U}_1$ and $\mathbf{U}_2$, and $\exp(t\Gamma) = \text{diag}\{\exp(\gamma_1 t), \exp(\gamma_2 t)\}$.

$$\mathbf{A} \equiv \begin{bmatrix} -(k_{01} + k_{21}[M]) & k_{12} \\ k_{21}[M] & -(k_{02} + k_{12}) \end{bmatrix} \tag{2}$$

$\mathbf{b}(\lambda^{ex})$ is the 2×1 vector of the excited-state concentrations at time zero,

$$\mathbf{b} \equiv = \begin{bmatrix} b_1 \\ b_2 \end{bmatrix} \equiv \begin{bmatrix} [1^*](0) \\ [2^*](0) \end{bmatrix}. \tag{3}$$

Note that $\mathbf{b}$ is dependent on the excitation wavelength λ^{ex} and [M].

$\mathbf{c}(\lambda^{em})$ is the 1×2 vector of the spectral emission weighting factors $c_i(\lambda^{em})$,

$$c_i(\lambda^{em}) = k_{Fi} \int_{\Delta\lambda^{em}} \rho_i(\lambda^{em})\, d\lambda^{em}. \tag{4}$$

k_{Fi} is the fluorescence rate constant of species i*; $\Delta\lambda^{em}$ is the emission wavelength interval where the fluorescence is monitored; $\rho_i(\lambda^{em})$ is the spectral emission density of species i* at λ^{em} defined by

$$\rho_i(\lambda^{em}) = \frac{F_i(\lambda^{em})}{\int F_i(\lambda^{em})\, d\lambda^{em}}, \tag{5}$$

where the integration extends over the whole steady-state fluorescence spectrum F_i of species i*. Defining the normalized elements $\tilde{b}_i$ and $\tilde{c}_i$,

$$\tilde{b}_i = b_i/(b_1 + b_2) \quad \text{for} \quad i = 1, 2 \tag{6a}$$

$$\tilde{c}_i = c_i/(c_1 + c_2) \quad \text{for} \quad i = 1, 2. \tag{6b}$$

Equation 1 can be written as

$$f(\lambda^{em}, \lambda^{ex}, t) = \kappa\tilde{\mathbf{c}}(\lambda^{em})\mathbf{U}\exp(t\Gamma)\mathbf{U}^{-1}\tilde{\mathbf{b}}(\lambda^{ex}), \quad t \geq 0 \tag{7}$$

with κ a proportionality constant. $\tilde{\mathbf{b}}(\lambda^{ex})$ can be linked over decay curves collected at the same excitation wavelength and

[M], whereas $\tilde{\mathbf{c}}(\lambda^{em})$ can be linked over decay curves obtained at the same emission wavelength.

Equation 7 can be written as a sum of two exponential terms:

$$f(\lambda^{em}, \lambda^{ex}, t) = \alpha_1(\lambda^{em}, \lambda^{ex})\exp(\gamma_1 t) + \alpha_2(\lambda^{em}, \lambda^{ex})\exp(\gamma_2 t), \quad t \geq 0 \quad (8)$$

The exponential factors $\gamma_{1,2}$ are given by

$$\gamma_{1,2} = -\tfrac{1}{2}\{X_1 + X_2 \pm [(X_1 - X_2)^2 + 4k_{21}k_{12}[M]]^{1/2}\} \quad (9)$$

and are related to the decay times $\tau_{1,2}$ according to

$$\gamma_{1,2} = -1/\tau_{1,2}, \quad (10)$$

with

$$X_1 = k_{01} + k_{21}[M] \quad (11a)$$

$$X_2 = k_{02} + k_{12}. \quad (11b)$$

For clarity, we shall not use the notation τ_1 and τ_2 but we shall refer to τ_L (L for long) and τ_S (S for short) with $\tau_L > \tau_S$.

The contribution of species i to the steady-state excitation spectrum $E(\lambda^{em}, \lambda^{ex}, [M])$ at [M], recorded at λ^{em} due to excitation at λ^{ex} is called the species-associated excitation spectrum of species i, $SAEXS_i(\lambda^{em}, \lambda^{ex})$, and is given by (Ameloot et al., 1991)

$$SAEXS_i(\lambda^{em}, \lambda^{ex}, [M]) = \frac{(\tilde{\mathbf{c}}(\lambda^{em})\mathbf{A}^{-1})_i\tilde{\mathbf{b}}_i(\lambda^{ex}, [M])}{\tilde{\mathbf{c}}(\lambda^{em})\mathbf{A}^{-1}\tilde{\mathbf{b}}(\lambda^{ex}, [M])} E(\lambda^{em}, \lambda^{ex}, [M]). \quad (12)$$

The contribution of species i* to the steady-state emission spectrum $F(\lambda^{em}, \lambda^{ex}, [M])$ at [M], recorded at λ^{em} due to excitation at λ^{ex} is called the species-associated emission spectrum of species i*, $SAEMS_i(\lambda^{em}, \lambda^{ex})$, and is given by (Ameloot et al., 1991):

$$SAEMS_i(\lambda^{em}, \lambda^{ex}, [M]) = \frac{\tilde{\mathbf{c}}_i(\lambda^{em})(\mathbf{A}^{-1}\tilde{\mathbf{b}}(\lambda^{ex}, [M]))_i}{\tilde{\mathbf{c}}(\lambda^{em})\mathbf{A}^{-1}\tilde{\mathbf{b}}(\lambda^{ex}, [M])} F(\lambda^{em}, \lambda^{ex}, [M]). \quad (13)$$

Fluorimetric titration

For the compartmental system depicted in Scheme 1, the measured steady-state fluorescence signal $F(\lambda^{em}, \lambda^{ex}, [M])$ due to excitation at λ^{ex} and observed at λ^{em} is given by (Ameloot et al., 1991)

$$F(\lambda^{em}, \lambda^{ex}, [M]) = -\xi(\lambda^{em})\mathbf{c}(\lambda^{em})\mathbf{A}^{-1}\mathbf{b}(\lambda^{ex}, [M]), \quad (14)$$

where $\xi(\lambda^{em})$ is an instrumental factor. If Beer's law is obeyed and if the absorbance of the solution is low (<0.1), then the elements $b_i(\lambda^{ex}, [M])$ of $\mathbf{b}$ can be approximated as

$$b_i(\lambda^{ex}, [M]) \approx 2.3d\epsilon_i(\lambda^{ex})[i]I_0(\lambda^{ex}), \quad (15)$$

where d denotes the excitation light path, $I_0(\lambda^{ex})$ represents the concentration (in mol/l) of excitation photons of wavelength λ^{ex} impinging on the sample, and $\epsilon_i(\lambda^{ex})$ is the molar extinction coefficient of species i at excitation wavelength λ^{ex}.

In the absence of an excited-state reaction

Without an excited-state reaction the compartmental matrix $\mathbf{A}$ is given by

$$\mathbf{A} \equiv \begin{bmatrix} -k_{01} & 0 \\ 0 & -k_{02} \end{bmatrix}. \quad (16)$$

If the absorbance of the solution is low, then Eq. 14 is explicitly given by

$$F(\lambda^{em}, \lambda^{ex}, [M]) = 2.3dI_0(\lambda^{ex})\xi(\lambda^{em})\{a_1(\lambda^{em})\epsilon_1(\lambda^{ex})[1] + a_2(\lambda^{em})\epsilon_2(\lambda^{ex})[2]\}, \quad (17)$$

$a_1(\lambda^{em})$ and $a_2(\lambda^{em})$ are defined by

$$a_1(\lambda^{em}) \equiv \frac{c_1(\lambda^{em})}{k_{01}} \quad (18a)$$

$$a_2(\lambda^{em}) \equiv \frac{c_2(\lambda^{em})}{k_{02}}. \quad (18b)$$

Expressing the ground-state dissociation constant K_d in the form of molar concentrations

$$K_d = \frac{[1][M]}{[2]} \quad (19)$$

and using the total analytical concentration, $C_T = [1] + [2]$ of the fluorescent probe allows us to rewrite Eq. 17 as

$$F(\lambda^{em}, \lambda^{ex}, [M]) = 2.3dI_0(\lambda^{ex})\xi(\lambda^{em})\frac{a_1\epsilon_1K_d + a_2\epsilon_2[M]}{K_d + [M]}C_T, \quad (20)$$

with $a_{1,2}$ defined by Eq. 18. The plot of F vs. $-\log[M]$ exhibits a unique inflection point at $[M] = K_d$. Equation 20 can be rewritten in the form of a Hill plot:

$$\log\left(\frac{F - F_{min}}{F_{max} - F}\right) = \log[M] - \log K_d. \quad (21)$$

Equation 20 indicates that the measured fluorescence signal F depends on C_T, I_0, and ξ. Most modern fluorimeters have the capability to correct for fluctuations of F due to I_0 by measuring simultaneously F and I_0 and computing/displaying the ratio F/I_0. If C_T, I_0, and ξ are constant during the measurement of samples with different [M], Eq. 20 constitutes the basis for fluorimetric titrations. In all other cases, the ratio method has to be used.

The ratio method can be performed in two ways. For each concentration of M one can either measure the ratio $R(\lambda^{em}, \lambda_1^{ex}/\lambda_2^{ex}, [M]) = F(\lambda^{em}, \lambda_1^{ex}, [M])/F(\lambda^{em}, \lambda_2^{ex}, [M])$ at two different excitation wavelengths and at a common emission wavelength, or the ratio $R(\lambda_1^{em}/\lambda_2^{em}, \lambda^{ex}, [M]) = F(\lambda_1^{em}, \lambda^{ex}, [M])/F(\lambda_2^{em}, \lambda^{ex}, [M])$ at two different emission wavelengths due to excitation at a single wavelength.

The ratio R obtained from dual excitation wavelengths at a common observation wavelength is given by Eq. 22

$$R(\lambda^{em}, \lambda_1^{ex}/\lambda_2^{ex}, [M]) = \left(\frac{S_1(\lambda^{em}, \lambda_1^{ex})K_d + S_2(\lambda^{em}, \lambda_1^{ex})[M]}{S_1(\lambda^{em}, \lambda_2^{ex})K_d + S_2(\lambda^{em}, \lambda_2^{ex})[M]}\right)\left(\frac{I_0(\lambda_1^{ex})}{I_0(\lambda_2^{ex})}\right), \quad (22)$$

where

$$S_i(\lambda^{em}, \lambda_j^{ex}) = a_i(\lambda^{em})\epsilon_i(\lambda_j^{ex}). \quad (23)$$

Equation 22 indicates that R is independent of the total concentration C_T. The dependence on I_0 can be eliminated by measuring directly F/I_0.

The plot of R as a function of $-\log[M]$ has a unique inflection point at $[M] = K_d S_1(\lambda^{em}, \lambda_2^{ex})/S_2(\lambda^{em}, \lambda_2^{ex})$. It must be emphasized that the ratio $S_1(\lambda^{em}, \lambda_2^{ex})/S_2(\lambda^{em}, \lambda_2^{ex})$ must be known in order to determine K_d. This ratio is determined by fluorescence measurements of the same system at the indicated wavelengths using extreme values of [M]: $F_{min}(\lambda^{em}, \lambda_2^{ex}, [M] \rightarrow 0) \equiv 2.3dI_0(\lambda_2^{ex})\xi(\lambda^{em})S_1(\lambda^{em}, \lambda_2^{ex})C_T$ and $F_{max}(\lambda^{em}, \lambda_2^{ex}, [M] \rightarrow \infty) \equiv 2.3dI_0(\lambda_2^{ex})\xi(\lambda^{em})S_2(\lambda^{em}, \lambda_2^{ex})C_T$. If the observation wavelength is set at the iso-emissive point, the ratio $S_1(\lambda^{em}, \lambda_2^{ex})/S_2(\lambda^{em}, \lambda_2^{ex})$ simplifies to $\epsilon_1(\lambda_2^{ex})/\epsilon_2(\lambda_2^{ex})$.

An inappropriate choice of excitation and observation wavelengths can make R invariant with [M], thus inhibiting the determination of K_d. The ratio $R(\lambda^{em}, \lambda_1^{ex}/\lambda_2^{ex}, [M])$ is independent of [M] if

$$a_1(\lambda^{em})a_2(\lambda^{em})[\epsilon_1(\lambda_2^{ex})\epsilon_2(\lambda_1^{ex}) - \epsilon_1(\lambda_1^{ex})\epsilon_2(\lambda_2^{ex})] = 0. \quad (24)$$

This is the case when (i) one of the excited-state species does not emit at the observation wavelength λ^{em} ($a_1(\lambda^{em}) = 0$ or $a_2(\lambda^{em}) = 0$) or when (ii) $\epsilon_1(\lambda_1^{ex})/\epsilon_2(\lambda_1^{ex}) = \epsilon_1(\lambda_2^{ex})/\epsilon_2(\lambda_2^{ex})$, i.e., when the absorption spectra of ground-state species 1 and 2 have identical shapes.

Equation 22 can be rearranged to yield [M]

$$[M] = K_d\left(\frac{R - \dfrac{S_1(\lambda^{em}, \lambda_1^{ex})I_0(\lambda_1^{ex})}{S_1(\lambda^{em}, \lambda_2^{ex})I_0(\lambda_2^{ex})}}{\dfrac{S_2(\lambda^{em}, \lambda_1^{ex})I_0(\lambda_1^{ex})}{S_2(\lambda^{em}, \lambda_2^{ex})I_0(\lambda_2^{ex})} - R}\right)\left(\frac{S_1(\lambda^{em}, \lambda_2^{ex})}{S_2(\lambda^{em}, \lambda_2^{ex})}\right), \quad (25)$$

which can be written as

$$[M] = K_d\left(\frac{R - R_{min}}{R_{max} - R}\right)\left(\frac{S_1(\lambda^{em}, \lambda_2^{ex})}{S_2(\lambda^{em}, \lambda_2^{ex})}\right), \quad (26)$$

with $R_{max} = \epsilon_2(\lambda_1^{ex})I_0(\lambda_1^{ex})/\epsilon_2(\lambda_2^{ex})I_0(\lambda_2^{ex})$ for $[M] \gg K_d$ and $R_{min} = \epsilon_1(\lambda_1^{ex})I_0(\lambda_1^{ex})/\epsilon_1(\lambda_2^{ex})I_0(\lambda_2^{ex})$ for $[M] \ll K_d$.

Note that Eq. 26 is the same as the calibration equation developed by Grynkiewicz et al. (1985) with

$$S_{f1} = 2.3dI_0(\lambda_2^{ex})\xi(\lambda^{em})S_1(\lambda^{em}, \lambda_2^{ex})C_T = F_{min}(\lambda^{em}, \lambda_2^{ex})$$

and

$$S_{b2} = 2.3dI_0(\lambda_2^{ex})\xi(\lambda^{em})S_2(\lambda^{em}, \lambda_2^{ex})C_T = F_{max}(\lambda^{em}, \lambda_2^{ex}).$$

Equation 26 is often rearranged in the form of a Hill plot:

$$\log\left(\frac{R - R_{min}}{R_{max} - R}\right) = \log[M] - \log\left(K_d\frac{S_1(\lambda^{em}, \lambda_2^{ex})}{S_2(\lambda^{em}, \lambda_2^{ex})}\right). \quad (27)$$

The expression of the left side of Eq. 27 plotted vs. $\log[M]$ should give a straight line that intersects the abscissa at the value corresponding to $\log(K_d S_1(\lambda^{em}, \lambda_2^{ex})/S_2(\lambda^{em}, \lambda_2^{ex}))$. Most often this plot is used to determine K_d provided $S_1(\lambda^{em}, \lambda_2^{ex})/S_2(\lambda^{em}, \lambda_2^{ex})$ is known.

The ratio R at dual emission wavelengths due to a common excitation wavelength is expressed by

$$R(\lambda_1^{em}/\lambda_2^{em}, \lambda^{ex}, [M]) = \left(\frac{S_1(\lambda_1^{em}, \lambda^{ex})K_d + S_2(\lambda_1^{em}, \lambda^{ex})[M]}{S_1(\lambda_2^{em}, \lambda^{ex})K_d + S_2(\lambda_2^{em}, \lambda^{ex})[M]}\right)\left(\frac{\xi(\lambda_1^{em})}{\xi(\lambda_2^{em})}\right), \quad (28)$$

with

$$S_i(\lambda_j^{em}, \lambda^{ex}) = a_i(\lambda_j^{em})\epsilon_i(\lambda^{ex}). \quad (29)$$

The plot of R vs. $-\log[M]$ has an inflection point at $[M] = K_d S_1(\lambda_2^{em}, \lambda^{ex})/S_2(\lambda_2^{em}, \lambda^{ex})$. The ratio $R(\lambda_1^{em}/\lambda_2^{em}, \lambda^{ex}, [M])$ becomes independent of [M] when

$$\epsilon_1(\lambda^{ex})\,\epsilon_2(\lambda^{ex})[a_1(\lambda_2^{em})\,a_2(\lambda_1^{em}) - a_1(\lambda_1^{em})\,a_2(\lambda_2^{em})] = 0. \quad (30)$$

This situation occurs when (i) one of the ground-state species does not absorb at the excitation wavelength λ^{ex} ($\epsilon_1(\lambda^{ex}) = 0$, $\epsilon_2(\lambda^{ex}) = 0$) or when (ii) $c_1(\lambda_1^{em})/c_2(\lambda_1^{em}) = c_1(\lambda_2^{em})/c_2(\lambda_2^{em})$, i.e., when the fluorescence spectra of excited-state species 1* and 2* have identical shapes.

Equation 28 can be transformed to give [M]

$$[M] = K_d\left(\frac{R - R_{min}}{R_{max} - R}\right)\left(\frac{S_1(\lambda_2^{em}, \lambda^{ex})}{S_2(\lambda_2^{em}, \lambda^{ex})}\right), \quad (31)$$

with $R_{max} = c_2(\lambda_1^{em})\xi(\lambda_1^{em})/c_2(\lambda_2^{em})\xi(\lambda_2^{em})$ for $[M] \gg K_d$ and $R_{min} = c_1(\lambda_1^{em})\xi(\lambda_1^{em})/c_1(\lambda_2^{em})\xi(\lambda_2^{em})$ for $[M] \ll K_d$.

Equation 31 also can be written in the form of a Hill plot

$$\log\left(\frac{R - R_{min}}{R_{max} - R}\right) = \log[M] - \log\left(K_d\frac{S_1(\lambda_2^{em}, \lambda^{ex})}{S_2(\lambda_2^{em}, \lambda^{ex})}\right). \quad (32)$$

This Hill plot intersects the abscissa at the value corresponding to $\log(K_d S_1(\lambda_2^{em}, \lambda^{ex})/S_2(\lambda_2^{em}, \lambda^{ex}))$.

In the presence of an excited-state reaction

In this case (Scheme 1) the compartmental matrix **A** is given by Eq. 2. The excited-state reaction will cause redistribution of excited states and consequently the fluorescence signal originating from each excited-state species will no longer be proportional to the number of photons absorbed by the corresponding ground-state species. In this case $F(\lambda^{em}, \lambda^{ex}, [M])$ is given by Eq. 17 or 20 with the coefficients $a_{1,2}(\lambda^{em})$ defined by

$$a_1(\lambda^{em}) \equiv \frac{c_1(\lambda^{em})(k_{02} + k_{12}) + c_2(\lambda^{em})k_{21}[M]}{k_{01}(k_{02} + k_{12}) + k_{02}k_{21}[M]} \quad (33a)$$

$$a_2(\lambda^{em}) \equiv \frac{c_1(\lambda^{em})k_{12} + c_2(\lambda^{em})(k_{01} + k_{21}[M])}{k_{01}(k_{02} + k_{12}) + k_{02}k_{21}[M]}. \quad (33b)$$

Whether or not there is excited-state reaction, F is formally described by Eq. 17 or 20 but with one significant difference. Indeed, the coefficients $a_{1,2}$ do not depend on [M] when there is no excited-state reaction (Eq. 18), whereas they do when there is an excited-state reaction (Eq. 33).

It has been shown (Kowalczyk et al., 1994) that the coefficients $a_{1,2}$ given by Eq. 33 are virtually independent of [M] except in the concentration range around [M] given by Eq. 34

$$[M] = \frac{k_{01}(k_{02} + k_{12})}{k_{02}k_{21}}. \quad (34)$$

If [M] given by Eq. 34 is quite different from K_d, the inflection point in the fluorimetric titration due to the ground-state equilibrium will occur at $[M] = K_d$. This implies that the excited-state reaction does not interfere with the determination of [M] and that Eq. 26 can be used.

The ratio of the fluorescence signals at two different excitation wavelengths and a common emission wavelength, $R(\lambda^{em}, \lambda_1^{ex}/\lambda_2^{ex}, [M])$ in the presence of an excited-state reaction is given by Eqs. 22 and 23 with $a_i(\lambda^{em})$ given by Eq. 33. At dual emission wavelengths and a common excitation wavelength the ratio $R(\lambda_1^{em}/\lambda_2^{em}, \lambda^{ex}, [M])$ of the fluorescence signals is given by Eqs. 28 and 29 with $a_i(\lambda^{em})$ given by Eq. 33. In general, the functional dependence of $R(\lambda^{em}, \lambda_1^{ex}/\lambda_2^{ex}, [M])$ and $R(\lambda_1^{em}/\lambda_2^{em}, \lambda^{ex}, [M])$ on $-\log[M]$ is very complicated and cannot be used to determine K_d. The ratios R_{min} and R_{max}, however, remain independent of the presence or absence of an excited-state reaction. The knowledge of all rate constants enables one to calculate a_i according to Eq. 33 and, consequently, to determine the concentration range of M where the interference of the excited-state reaction is insignificant.

MATERIALS AND METHODS

Materials

Fura-2, pentapotassium salt was obtained from Molecular Probes (Eugene, OR). EGTA (ethylene glycol-bis(β-aminoethyl ether) *N,N,N′,N′*-tetraacetic acid), BAPTA (1,2-bis(2-aminophenoxy)ethane-*N,N,N′,N′*-tetraacetic acid), and MOPS (3-(*N*-morpholino)propanesulfonic acid) Free Acid were purchased from Sigma Chemie (Bornem, Belgium). KCl and $CaCl_2$ were obtained from Janssen Chimica (Geel, Belgium). All of these products were used without further purification. Milli-Q water was used to prepare the aqueous solutions according to the procedure described by Grynkiewicz et al (1991). Free [Ca^{2+}] levels were controlled either by Ca^{2+}/BAPTA buffers assuming a dissociation constant of 130 nM for the Ca^{2+}/BAPTA complex or by Ca^{2+}/EGTA buffers assuming a dissociation constant of 151 nM for the Ca^{2+}/EGTA complex both at pH 7.2 in 100 mM KCl aqueous solution at room temperature. The dissociation constants of the Ca^{2+}/BAPTA and Ca^{2+}/EGTA complexes calculated according to Marks and Maxfield (1991) were used to determine the free [Ca^{2+}]. The ionic strength of these solutions varied from 0.1 to 0.3. In a second set of experiments, KCl was used to adjust the ionic strength of each solution to a constant value of 0.3.

Instrumentation

Fully corrected steady-state excitation and emission spectra were recorded on a SPEX Fluorolog 212. The fluorescence decay traces were measured by the single photon timing technique using the synchrotron radiation machine SUPER-ACO (Anneau de Collision d'Orsay at LURE, France) as described elsewhere (Kuipers et al., 1991). The polarization of the excitation beam was vertical with respect to the excitation-emission plane. The total fluorescence decay was constructed from the polarized fluorescence intensity decays collected with the polarizer in the emission path set parallel and perpendicular with respect to the excitation polarization and taking into account the polarization bias of the instrument. The storage ring provides a light pulse with a full width at half maximum of ≈500 ps at a frequency of 8.33 MHz in double-bunch mode. A Hamamatsu microchannel plate R1564U-06 was used to detect the fluorescence photons. The instrument response function was determined by measuring the light scattered by glycogen in aqueous solution at the emission wavelength and was collected alternately with the parallel and perpendicular components of the polarized fluorescence decay. All decay traces were collected in ½K channels of a multichannel analyzer and contained approximately 5×10^3 peak counts. The time increment per channel was 12 ps.

Data analysis

The global compartmental analysis of the fluorescence decay surface of species undergoing excited-state processes was implemented in the existing general global analysis program (Boens et al., 1989) based on Marquardt's (1963) algorithm. Our implementation of global compartmental analysis, which is an extension of that described by Beechem et al. (1985), allows unnormalized decay curves to be used. The global fitting parameters are k_{01}, k_{21}, k_{02}, k_{12}, $\tilde{b}_1$, and $\tilde{c}_1$. The rate constants k_{01}, k_{21}, k_{02}, and k_{12} are the same for all decays. In contrast, the coefficients $\tilde{c}_1$ are expected to be identical only for those decays observed at the same emission wavelength. The normalized ground-state absorbances $\tilde{b}_1$ are identical for the decays at the same excitation wavelength and Ca^{2+} concentration. This knowledge about internal links between the fitting parameters of the decay curves constituting the fluorescence decay surface is presented graphically in Scheme 2. In that scheme boxed parameters represent linked parameters, and X denote local scaling factors.

Specifying the Ca^{2+} concentration and assigning initial guesses to the rate constants k_{01}, k_{21}, k_{02}, and k_{12} allows one to construct the compartmental

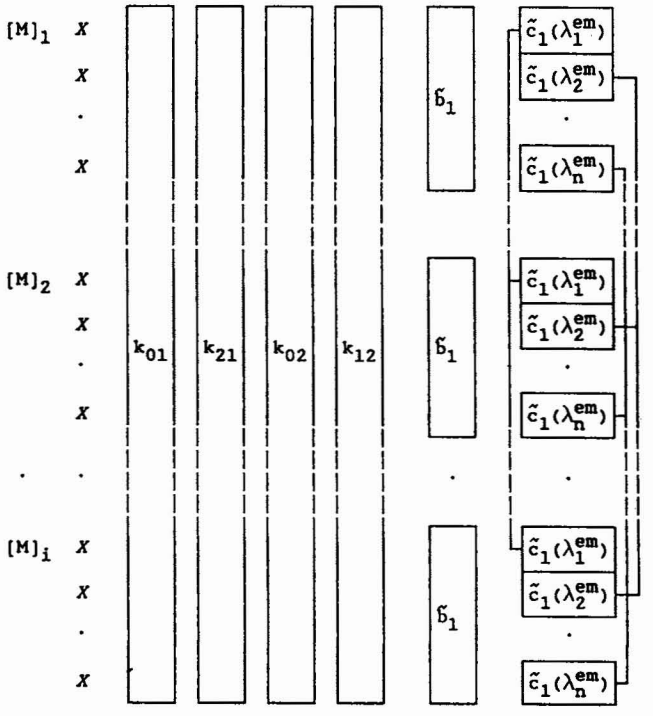

Scheme 2

matrix **A** (Eq. 2) for each decay trace. The eigenvalues γ and the associated eigenvectors **U** of this matrix are determined using routines from EISPACK, Matrix Eigensystem Routines (Smith et al., 1974). The eigenvectors are then scaled to the initial conditions $\bar{b}$. The preexponential factors α are computed from the rate constants, $[Ca^{2+}]$, $\bar{b}$, and $\bar{c}$, allowing the calculation of the fluorescence decay of the sample. Using this approach, all decay traces collected at different excitation/emission wavelengths, at multiple timing calibrations, and at different Ca^{2+} concentrations are linked by all rate constants defining the system and can therefore be analyzed simultaneously by the model given by Eq. 7.

The fitting parameters were determined by minimizing the *global reduced* chi-square χ_g^2:

$$\chi_g^2 = \sum_l^q \sum_i w_{li}(y_{li}^o - y_{li}^c)^2/v, \tag{35}$$

where the index l sums over q experiments, and the index i sums over the appropriate channel limits for each individual experiment. y_{li}^o and y_{li}^c denote respectively the observed (experimentally measured) and fitted values corresponding to the ith channel of the lth experiment. w_{li} is the corresponding statistical weight taking into account the construction of y_{li}^o from the polarized intensity decays (Boens, 1991). v represents the number of degrees of freedom for the entire multidimensional fluorescence decay surface. The statistical criteria to judge the quality of the fit comprised both graphical and numerical tests. The graphical methods included plots of surfaces ("carpets") of the autocorrelation function values versus experiment number, and of the weighted residuals versus channel number versus experiment number. The global reduced chi-square statistic χ_g^2 and its corresponding $Z_{\chi_g^2}$ provided numerical goodness-of-fit criteria for the entire fluorescence decay surface.

$$Z_{\chi_g^2} = (\chi_g^2 - 1)\sqrt{\tfrac{1}{2}v}. \tag{36}$$

Using $Z_{\chi_g^2}$ the goodness-of-fit of analyses with different v can be readily compared. Moreover, the goodness-of-fit was examined for the individual decay curves by the calculation of the ordinary runs test, the Durbin-Watson statistic, the local χ^2 value χ_l^2 and its normal deviate $Z_{\chi_l^2}$ (Boens, 1991). SE estimates were obtained from the parameter covariance matrix available from the analysis. All quoted errors are one standard deviation. All analyses were done on an IBM RISC System/6000 computer.

RESULTS

The ground-state dissociation constant K_d of the Ca^{2+}/Fura-2 complex was determined from a Hill plot using absorption measurements at λ^{ex} = 340 nm, at 20°C, pH 7.2, and 100 mM KCl in aqueous solution with EGTA as Ca^{2+} buffer. The Hill plot yielded a value of 134 (±11) nM for K_d (corresponding to pK_d = 6.87) and indicated a 1:1 stoichiometry for the Ca^{2+}/Fura-2 complex. The dissociation constant in the excited-state, K_d^*, can be calculated according to the Förster cycle (Weller, 1961):

$$pK_d^* = pK_d - \frac{\Delta E_2 - \Delta E_1}{2.303RT}, \tag{37}$$

where ΔE_1 is the 0–0 transition energy of the free form and ΔE_2 the corresponding 0–0 transition energy of the bound form of the indicator. Because of the broad absorption and emission spectra, it is impossible to determine the 0–0 transitions. To overcome this difficulty, the difference $(\Delta E_2 - \Delta E_1)$ was calculated by averaging the frequencies of absorption and fluorescence maxima of both the Ca^{2+} free and bound forms of the indicator. This resulted in a pK_d^* of 4.

To determine the excited-state parameters, time-resolved fluorescence measurements were performed. With BAPTA as Ca^{2+} buffer decay curves of Fura-2 at different concentrations of Ca^{2+} ranging from 101 nM to 0.1 M were measured at two different excitation wavelengths (λ^{ex} = 350 nm, 370 nm) and two different emission wavelengths (λ^{em} = 490 nm, 510 nm). When EGTA was used as Ca^{2+} buffer, the two excitation wavelengths were 340 and 370 nm, whereas the other experimental conditions were identical. In both cases no extra salt was added to keep the ionic strength constant.

The decays arising from solutions with identical Ca^{2+} concentrations were analyzed globally as biexponential functions in terms of preexponential factors and decay times (Eq. 8) with the latter being linked over the emission and excitation wavelengths at each concentration of Ca^{2+}. Biexponential global analysis gave good fits over the whole concentration range even at Ca^{2+} concentrations of 5×10^{-5} M or higher, when the indicator is saturated in the ground state. The estimated decay times are shown in Table 1. From this table it is clear that for increasing $[Ca^{2+}]$ the shorter decay time decreases whereas the longer decay time increases. The only detailed information on the rate constants that can be derived from this observations is that $k_{02} < k_{01}$.

In global compartmental analysis, all the decays were analyzed simultaneously according to linking Scheme 2. The resulting rate constants are shown in Table 2. It is noteworthy that good fits were only obtained when Ca^{2+} concentrations and not activities were entered into the program. It must be emphasized that all solutions—even those at high Ca^{2+} concentration—had to contain BAPTA or EGTA to obtain an acceptable fit for the global compartmental analysis. It was only when all solutions were prepared with the same total BAPTA or EGTA concentration that an acceptable fit was obtained for all the decays at all Ca^{2+} concentrations. The results of Table 2 indicate that k_{01} and k_{02} are independent of the Ca^{2+} buffer used. The values of k_{12} and k_{21}, however, are clearly dependent on the Ca^{2+} buffer: they are apparent rate constant values. Beside the interconversion of the Ca^{2+} free

TABLE 1 Globally estimated decay times of Fura-2 at different ionic strength as a function of Ca^{2+} concentration

$[Ca^{2+}]$	τ_L (ns)	τ_S (ns)	#*	χ_g^2	$Z_{\chi_g^2}$
A. BAPTA as Ca^{2+} buffer					
101 nM	1.691 (±0.004)	0.777 (±0.004)	3	1.08	2.48
604 nM	1.755 (±0.003)	0.799 (±0.004)	4	1.10	4.35
5×10^{-5} M	1.804 (±0.003)	0.807 (±0.005)	4	1.05	2.13
5×10^{-4} M	1.795 (±0.009)	0.807 (±0.007)	4	1.09	2.38
10^{-3} M	1.794 (±0.008)	0.691 (±0.006)	4	1.12	3.21
10^{-2} M	1.822 (±0.001)	0.44 (±0.02)	4	1.05	2.04
0.1 M	1.867 (±0.004)	0.30 (±0.02)	4	1.08	2.41
B. EGTA as Ca^{2+} buffer					
101 nM	1.717 (±0.003)	0.684 (±0.003)	4	1.10	4.82
604 nM	1.683 (±0.003)	0.684 (±0.003)	4	1.10	4.12
5×10^{-5} M	1.722 (±0.003)	0.713 (±0.004)	4	1.11	3.30
5×10^{-4} M	1.784 (±0.002)	0.691 (±0.003)	4	1.08	3.38
10^{-3} M	1.801 (±0.006)	0.631 (±0.002)	4	1.06	3.21
10^{-2} M	1.819 (±0.003)	0.50 (±0.01)	4	1.05	2.44
0.1 M	1.870 (±0.002)	0.41 (±0.01)	4	1.14	5.21

*Number of decays analyzed simultaneously.

TABLE 2 Rate constant values of Fura-2 estimated by global compartmental analysis from decay traces at different ionic strength

Rate constant	BAPTA as Ca^{2+} buffer	EGTA as Ca^{2+} buffer
k_{01} $(ns)^{-1}$	1.239 (±0.004)	1.424 (±0.003)
k_{21} $(M\ ns)^{-1}$	103 (±7)	50 (±4)
k_{02} $(ns)^{-1}$	0.5509 (±0.0008)	0.549 (±0.001)
k_{12} $(ns)^{-1}$	0.022 (±0.003)	0.032 (±0.001)

and bound forms of Fura-2 in the excited state (Scheme 1, Eq. 38a), reactions of excited Fura-2 with Ca^{2+}:EGTA (Eqs. 38b-c) and Ca^{2+}:BAPTA (Eq. 38d) complexes must be included in the reaction scheme (Marks and Maxfield, 1991).

$$\text{Fura-2}^* + Ca^{2+} \rightleftarrows [\text{Ca:Fura-2}^*]^{2+} \tag{38a}$$

$$\text{Fura-2}^* + \text{CaEGTA}^{2-} \rightleftarrows [\text{Ca:Fura-2}^*]^{2+} + \text{EGTA}^{4-} \tag{38b}$$

$$\text{Fura-2}^* + \text{CaHEGTA}^{-} \rightleftarrows [\text{Ca:Fura-2}^*]^{2+} + \text{HEGTA}^{3-} \tag{38c}$$

$$\text{Fura-2}^* + \text{CaBAPTA}^{2-} \rightleftarrows [\text{Ca:Fura-2}^*]^{2+} + \text{BAPTA}^{4-} \tag{38d}$$

Therefore, k_{21} and k_{12} describe not only the process of Eq 38a but all the above excited-state processes. The different values obtained for k_{21} and k_{12} with EGTA and BAPTA buffers reflect the different values of the individual rate constants. The occurrence of the excited-state processes given by Eqs. 38b–d may account for the fact that the same concentration of Ca^{2+} buffer had to be present in all solutions to obtain an acceptable fit in global compartmental analysis. From the obtained rate constants the decay times can be calculated as a function of $[Ca^{2+}]$ according to Eqs. 9–11. For BAPTA as Ca^{2+} buffer these decay times are plotted in Fig. 1 as a function of $-\log[Ca^{2+}]$ together with the decay times estimated directly from global biexponential analysis. It is clear that there is a good agreement between the decay times estimated directly from standard global biexponential analysis and those calculated using the rate constant values from global compartmental analysis. Similar results were obtained for EGTA as Ca^{2+} buffer (results not shown).

For the estimation of the rate constants of Table 2, solutions of Fura-2 with high Ca^{2+} concentrations (up to 0.1 M) were used. Obviously, the ionic strength of the solutions with high $[Ca^{2+}]$ is much higher than that of solutions with low Ca^{2+} concentration. To check whether the decay times are sensitive to the change in ionic strength, decay curves of solutions with the same ionic strength (I = 0.3) were measured with BAPTA as Ca^{2+} buffer. As in the previous experiments, the Ca^{2+} concentration was varied from 101 nM to 0.1 M. The decays arising from solutions with identical Ca^{2+} concentrations were analyzed globally as biexponentials as before. Biexponential global analysis gave good fits for all Ca^{2+} concentrations. The estimated decay times (Fig. 2) as a function of $-\log[Ca^{2+}]$ are virtually the same as in Fig. 1. Therefore, the ionic strength can be excluded as an experimental variable influencing the decay times and the rate constant values. The normalized preexponential factors at λ^{ex} = 350 nm and λ^{em} = 490 nm corresponding to the long decay time $\alpha_L/(\alpha_S + \alpha_L)$ as a function of $-\log[Ca^{2+}]$ are shown in Fig. 3. It is clear that the ionic strength has a minor effect on the preexponential factors. Similar plots were obtained at other excitation and/or emission wavelengths. Therefore, the ionic strength influences minimally the binding of Ca^{2+} by Fura-2.

From the values for k_{01}, k_{02}, and the quantum yields of fluorescence, Q for the Ca^{2+} free and bound forms of Fura-2, the respective radiative deactivation rate constants can be calculated. According to Grynkiewicz et al. (1991) the values for Q are 0.23 and 0.49 for the Ca^{2+} free and bound forms of Fura-2, respectively. Because k_{0i} comprises both radiative and nonradiative rate processes, the rate constants of nonradiative decay can also be calculated. Table 3 gives the rate

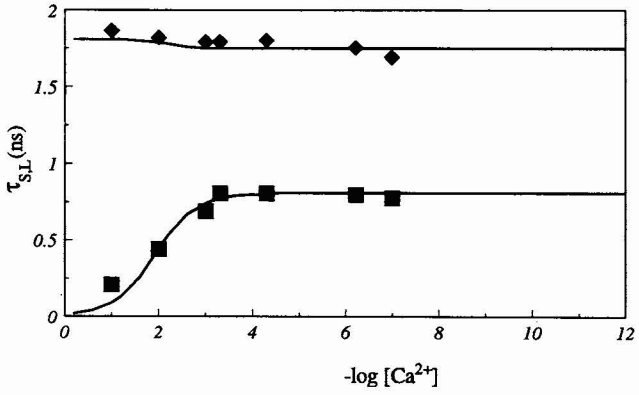

FIGURE 1 Decay times (——) of Fura-2 as a function of $-\log[Ca^{2+}]$ calculated according to Eqs. 9–11 with the rate constant values obtained from global compartmental analysis using BAPTA as Ca^{2+} buffer (Table 2). The symbols ■ and ◆ represent the decay times estimated from standard global biexponential analysis of solutions with unequal ionic strength.

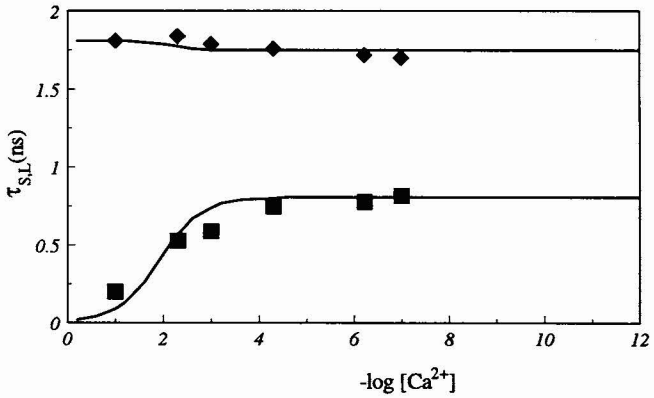

FIGURE 2 Decay times (——) of Fura-2 as a function of $-\log[Ca^{2+}]$ calculated according to Eqs. 9–11 with the rate constant values obtained from global compartmental analysis using BAPTA as Ca^{2+} buffer (Table 2). The symbols ■ and ◆ represent the decay times estimated from standard global biexponential analysis of solutions with high constant ionic strength (I = 0.3).

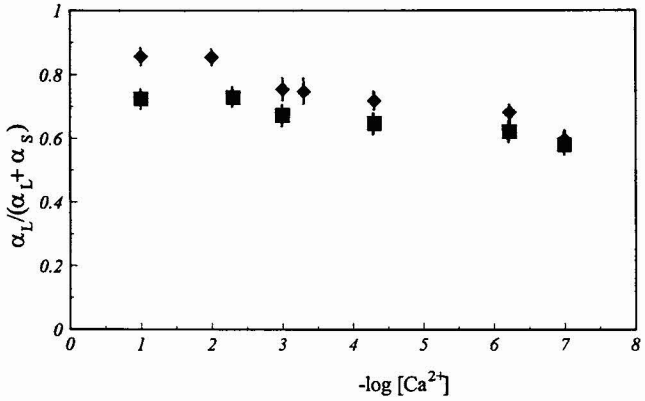

FIGURE 3 Normalized preexponential $\alpha_L/(\alpha_S + \alpha_L)$ obtained at λ^{ex} = 350 nm and λ^{em} = 490 nm as a function of $-\log[Ca^{2+}]$. α_L (respectively α_S) is the preexponential factor corresponding to τ_L (respectively τ_S). The symbols ♦ and ■ depict measurements at variable and constant ionic strength, respectively. BAPTA was used as Ca^{2+} buffer.

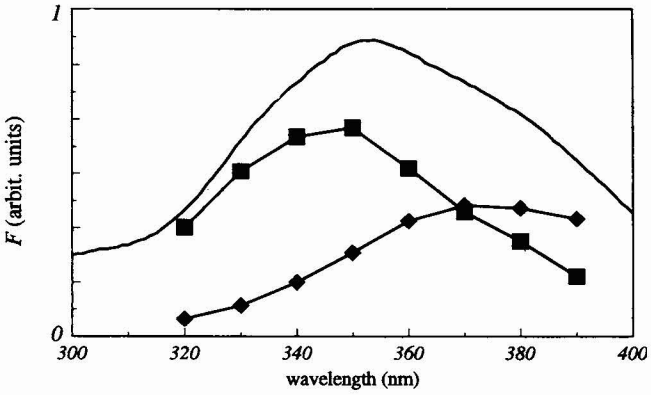

FIGURE 4 Decomposition of the measured steady-state excitation spectrum E (——) of Fura-2 into the SAEXS of the Ca^{2+} free form (–♦–) and Ca^{2+} bound form (–■–) at $[Ca^{2+}]$ = 226 nM and λ^{em} = 490 nm. EGTA was used as Ca^{2+} buffer.

constant values for fluorescence and nonradiative decay for the Ca^{2+} free and bound forms of Fura-2. The radiative rate constant is almost the same for both species, whereas the nonradiative processes are less important in the bound form. This accounts for the increase in the fluorescence intensity when the Ca^{2+} concentration is increased.

To construct the species-associated excitation spectra (SAEXS), decay curves of solutions with $[Ca^{2+}]$ = 226 nM and EGTA as Ca^{2+} buffer were collected at two different emission wavelengths (λ^{em} = 470 nm, 490 nm) due to excitation at different excitation wavelengths between 320 and 390 nm. BAPTA could not be used because it absorbs at wavelengths under 350 nm. Sixteen decays were included in one global compartmental analysis yielding a χ_g^2 value of 1.03 ($Z_{\chi_g^2}$ = 3.01). The SAEXS calculated according to Eq. 12 at λ^{em} = 490 nm are shown in Fig. 4. The SAEXS correspond very well with the excitation spectra of the Ca^{2+} free and bound forms of Fura-2 recorded separately (Grynkiewicz et al., 1985). Note that the pseudo-isosbestic point is at 370 nm (fig. 4) for detection at 490 nm. The usually reported wavelength for the pseudo-isosbestic point is 360 nm for detection at 510 nm (Grynkiewicz et al., 1991).

From k_{12}/k_{21} the dissociation constant K_d^* in the excited state can be calculated. This yields values for pK_d^* of 3.7 with BAPTA and 3.2 with EGTA as Ca^{2+} buffers. These values are in fair agreement with the result of the Förster cycle. This indicates that the excited state is more dissociative than the ground state.

TABLE 3 Radiative (k_F) and nonradiative (k_{NR}) deactivation rate constant values of the Ca^{2+} free and bound forms of Fura-2

Species	Q^*	k_F (ns)$^{-1}$	k_{NR} (ns)$^{-1}$
A. BAPTA as Ca^{2+} buffer			
Free (1)	0.23	0.28	0.96
Bound (2)	0.49	0.27	0.28
B. EGTA as Ca^{2+} buffer			
Free (1)	0.23	0.32	1.10
Bound (2)	0.49	0.27	0.28

*Values taken from Grynkiewicz et al. (1985).

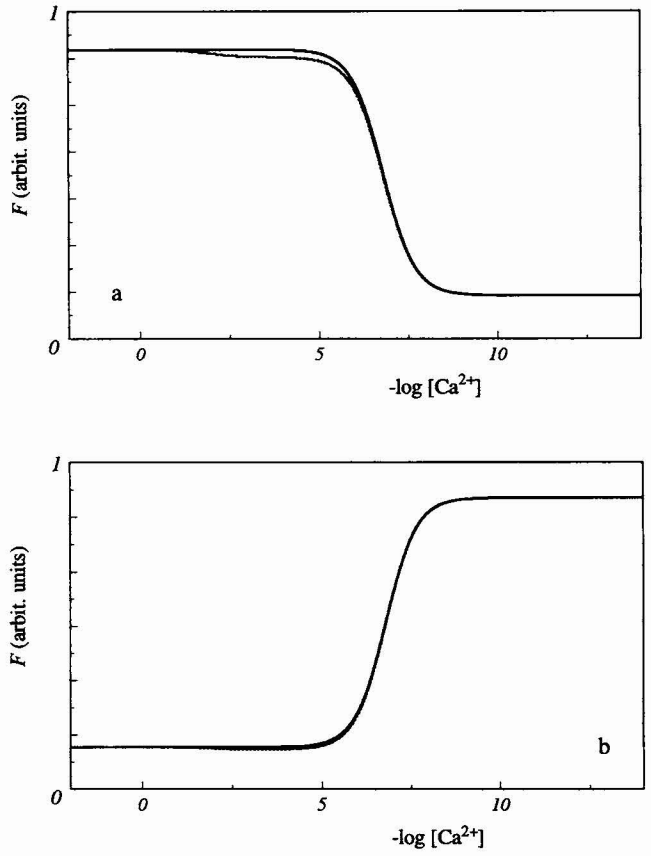

FIGURE 5 Fluorimetric titration curves F computed in the absence (——) and presence (-------) of an excited-state reaction at λ^{em} = 510 nm with λ^{ex} = 340 nm (a) and λ^{ex} = 380 nm (b). The rate constants of Table 2 for BAPTA as Ca^{2+} buffer were used together with the following experimentally determined values of K_d = 130 nM; ϵ_1 = 13,300 M^{-1} cm^{-1}, ϵ_2 = 29,900 M^{-1} cm^{-1} at λ^{ex} = 340 nm; ϵ_1 = 18300 M^{-1} cm^{-1}, ϵ_2 = 1700 M^{-1} cm^{-1} at λ^{ex} = 380 nm; $c_1/(c_1 + c_2)$ = 0.43, $c_2/(c_1 + c_2)$ = 0.57 at λ^{em} = 510 nm.

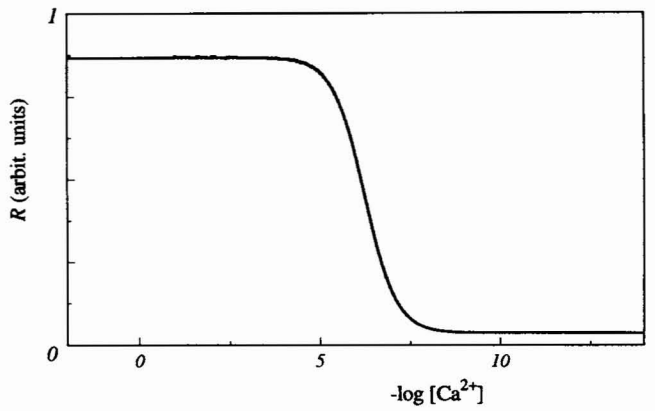

FIGURE 6 Fluorimetric titration curves $R = F(510\text{ nm}, 340\text{ nm})/F(510\text{ nm}, 380\text{ nm})$ computed according to Eqs. 22 and 23 with a_i given by Eq. 18 (without excited-state reaction) and Eq. 33 (with excited-state reaction) using the rate constants of Table 2 for BAPTA as Ca^{2+} buffer at $\lambda^{ex} = 340$ nm ($\epsilon_1 = 13300\ M^{-1}\ cm^{-1}$, $\epsilon_2 = 29900\ M^{-1}\ cm^{-1}$) and 380 nm ($\epsilon_1 = 18300\ M^{-1}\ cm^{-1}$, $\epsilon_2 = 1700\ M^{-1}\ cm^{-1}$), observed at $\lambda^{em} = 510$ nm($c_1/(c_1 + c_2) = 0.43$, $c_2/(c_1 + c_2) = 0.57$), $K_d = 130$ nM.

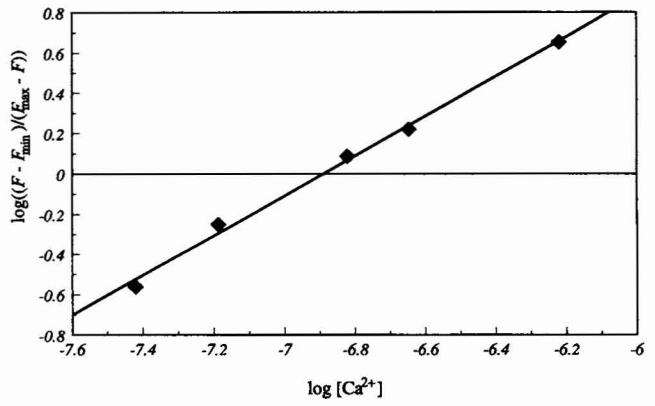

FIGURE 7 Hill plot (Eq. 21) of F for Fura-2 measured at $\lambda^{ex} = 340$ nm and observed at $\lambda^{em} = 510$ nm at pH 7.2 with EGTA as Ca^{2+} buffer in aqueous solution at room temperature.

The determined values for k_{01}, k_{02}, k_{12}, and k_{21} allow us to check whether the excited-state reaction interferes with the fluorimetric determination of the ground-state dissociation constant K_d. It is not generally acknowledged that the excited-state reaction can severely distort the values of K_d and/or $[Ca^{2+}]$ obtained from fluorimetric titrations. To investigate the interference of the excited-state reaction with the recovered value of K_d, fluorimetric titration curves F were computer-generated at two excitation wavelengths (340 and 380 nm) and a common observation wavelength (510 nm) assuming the presence or absence of an excited-state reaction. The rate constants for BAPTA as Ca^{2+} buffer (Table 2) were used together with the following experimentally determined values of $K_d = 130$ nM, $\epsilon_1 = 13300\ M^{-1}\ cm^{-1}$, and $\epsilon_2 = 29900\ M^{-1}\ cm^{-1}$ at $\lambda^{ex} = 340$ nm; $\epsilon_1 = 18300\ M^{-1}\ cm^{-1}$, $\epsilon_2 = 1700\ M^{-1}\ cm^{-1}$ at $\lambda^{ex} = 380$ nm; $c_1/(c_1 + c_2) = 0.43$, $c_2/(c_1 + c_2) = 0.57$ at $\lambda^{em} = 510$ nm. The resulting fluorimetric titration curves F vs. $-\log[Ca^{2+}]$ are shown in

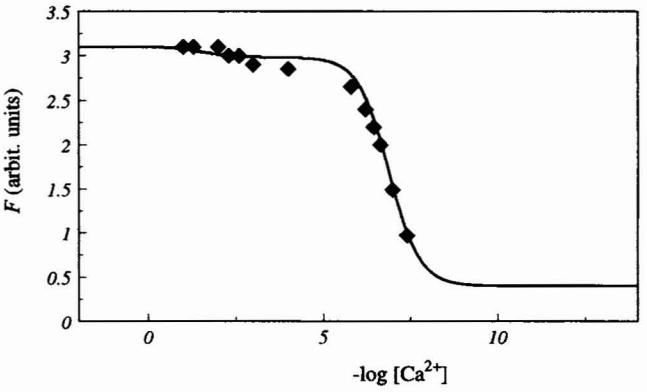

FIGURE 8 Experimental (◆) fluorimetric titration curve $F(510\text{ nm}, 340\text{ nm})$ for Fura-2 at pH 7.2 with EGTA as Ca^{2+} buffer in aqueous solution at room temperature. The solid line represents the $F(510\text{ nm}, 340\text{ nm})$ values calculated with $K_d = 130$ nM, $\epsilon_1 = 13300\ M^{-1}\ cm^{-1}$ and $\epsilon_2 = 29{,}900\ M^{-1}\ cm^{-1}$ at $\lambda^{ex} = 340$ nm; $c_1/(c_1 + c_2) = 0.43$, $c_2/(c_1 + c_2) = 0.57$ at $\lambda^{em} = 510$ nm. The used rate constants are those of Table 2 for EGTA as Ca^{2+} buffer.

Fig. 5, indicating that the inflection points are practically independent of the presence of an excited-state reaction. Note that the inflection points due to ground-state reaction occur at $[Ca^{2+}] = K_d$. Calculation of the Ca^{2+} concentration where the inflection point due to the excited-state reaction occurs (Eq. 34) also shows the negligible interference of the excited-state reaction on the determination of K_d. Indeed, according to Eq. 34, $-\log[Ca^{2+}] = 1.90$ when BAPTA is used as Ca^{2+} buffer and $-\log[Ca^{2+}] = 1.52$ when EGTA is used. As these inflection points are far removed from pK_d (6.87), the excited-state reaction does not influence the fluorimetric titrations. Therefore, fluorimetric titrations can be safely used to determine K_d and/or Ca^{2+} concentration.

The titration curves of Fig. 5 were used to calculate R in the absence and presence of an excited-state reaction. The calculated titration curves $R = F(510\text{ nm}, 340\text{ nm})/F(510\text{ nm}, 380\text{ nm})$ in the presence or absence of an excited-state reaction are shown in Fig. 6 and are indistinguishable. It must be emphasized that the inflection point occurs at a Ca^{2+} concentration different from K_d. Indeed, the titration curve R has an inflection point at $[Ca^{2+}] = K_d S_1(\lambda^{em}, \lambda_2^{ex})/S_2(\lambda^{em}, \lambda_2^{ex}) = K_d[\epsilon_1(\lambda_2^{ex})c_1(\lambda^{em})k_{02}]/[\epsilon_2(\lambda_2^{ex})c_2(\lambda^{em})k_{01}] = 478$ nM. Using the values of $\epsilon_1(380\text{ nm}) = 18300\ M^{-1}\ cm^{-1}$, $\epsilon_2(380\text{ nm}) = 1700\ M^{-1}\ cm^{-1}$, $c_1/(c_1 + c_2)$ at 510 nm = 0.43, $c_2/(c_1 + c_2)$ at 510 nm = 0.57, $k_{01} = 1.239 \times 10^9\ s^{-1}$ and $k_{02} = 0.5509 \times 10^9\ s^{-1}$, the ground-state dissociation constant K_d was calculated and found to be 132 nM. This value agrees excellently with the simulation value.

From the fluorimetric titration of Fura-2 in aqueous solution at pH 7.2 in the form of a Hill plot (Eq. 21) with EGTA as Ca^{2+} buffer (Fig. 7), a value of 129 (±5) nM was found for K_d in excellent agreement with the value of 134 (±11) nM obtained from absorbance measurements. These results confirm that the excited-state reaction does not interfere with the determination of K_d. The slope (0.99 ± 0.04) of the Hill plot indicates that Ca^{2+} binds to Fura-2 with a 1:1 stoichiometry. In Fig. 8 the experimental fluorimetric titration curve F

(340 nm, 510 nm) at pH 7.2 with EGTA as Ca^{2+} buffer is shown as a function of $-\log[Ca^{2+}]$ with $[Ca^{2+}]$ ranging from 38 nM to 0.1 M. The solid line represents the fluorescence signal calculated with K_d = 130 nM, ϵ_1 = 13300 M^{-1} cm^{-1} and ϵ_2 = 29900 M^{-1} cm^{-1} at λ^{ex} = 340 nm; $c_1/(c_1 + c_2)$ = 0.43, $c_2/(c_1 + c_2)$ = 0.57 at λ^{em} = 510 nm. The used rate constants are those of Table 2 for EGTA as Ca^{2+} buffer. There is an excellent agreement between the experimental and calculated fluorimetric titration curves. The inflection point due to the excited-state processes is hardly visible. Note that the calculated fluorimetric titration curves in the presence and absence of an excited-state binding reaction have an inflection point at K_d.

CONCLUSION

In this paper, we have investigated the reversible excited-state complex forming reaction of Ca^{2+} by Fura-2. Using global compartmental analysis, it was possible to determine all the rate constants of the excited-state reaction only when (i) Ca^{2+} concentrations and not activities were entered into the program and when (ii) the total Ca^{2+} buffer concentration was the same in all samples. The ionic strength of the solution was shown not to influence the recovered values of the rate constants. From the estimated values of k_{12} and k_{21} the dissociation constant K_d^* was calculated. It was found that pK_d^* is smaller than pK_d by more than three units. There is negligible interference of the excited-state reaction with the determination of K_d and $[Ca^{2+}]$ from fluorimetric titrations. Using the results from global compartmental analysis, the steady-state excitation spectrum could be decomposed into the excitation spectra associated with the Ca^{2+} free and bound forms of Fura-2.

V. Van den Bergh is a predoctoral fellow of the Belgian Instituut tot Aanmoediging van het Wetenschappelijk Onderzoek in de Nijverheid en de Landbouw (IWONL). N. Boens is an Onderezoeksleider of the Belgian Fonds voor Geneeskundig Wetenschappelijk Onderzoek (FGWO). The continuing support of the Ministry of Scientific Programming through IUAP-II-16 is gratefully acknowledged. A. Kowalczyk had an Individual E. C. Fellowship under the Community mobility action for Cooperation in Science and Technology with Central and Eastern European Countries which enabled him to stay at the K.U. Leuven. He also thanks the K.U. Leuven for the hospitality during his stay there.

REFERENCES

Ameloot, M., N. Boens, R. Andriessen, V. Van den Bergh, and F. C. De Schryver. 1991. Non a priori analysis of fluorescence decay surfaces of excited-state processes. 1. Theory. *J. Phys. Chem.* 95: 2041–2047.

Ameloot, M., N. Boens, R. Andriessen, V. Van den Bergh, and F. C. De Schryver. 1992. Compartmental analysis of fluorescence decay surfaces of excited-state processes. *Methods Enzymol.* 210:314–340.

Beechem, J. M., M. Ameloot, and L. Brand. 1985. Global analysis of fluorescence decay surfaces: excited-state reactions. *Chem. Phys. Lett.* 120: 466–472.

Boens, N. 1991: Pulse fluorometry. *In* Luminescence Techniques in Chemical and Biochemical Analysis. W. R. G. Baeyens, D. De Keukeleire, and K. Korkidis, editors. Marcel Dekker, New York. 21–45.

Boens, N., L. D. Janssens, and F. C. De Schryver. 1989. Simultaneous analysis of single-photon timing data for the one-step determination of activation energies, frequency factors and quenching rate constants. Application to tryptophan photophysics. *Biophys. Chem.* 33: 77–90.

Bush, D. S., and R. L. Jones. 1990. Measuring intracellular Ca^{2+} levels in plant cells using the fluorescent probes, Indo-1 and Fura-2. *Plant Physiol.* 93:841–845.

Cobbold, P. H., and T. J. Rink. 1987. Fluorescence and bioluminescence measurement of cytoplasmic free calcium. *Biochem. J.* 248:313–328.

Grynkiewicz, G., M. Poenie, and R. Y. Tsien. 1985. A new generation of Ca^{2+} indicators with greatly improved fluorescence properties. *J. Biol. Chem.* 260:3440–3450.

Iaizzo, P. A., M. Seewald, S. G. Oakes, and F. Lehmann-Horn. 1989. The use of Fura-2 to estimate myoplasmic $[Ca^{2+}]$ in human skeletal muscle. *Cell Calcium.* 10:151–158.

Keating, S., and T. G. Wensel. 1991. Nanosecond fluorescence microscopy. Emission kinetics of Fura-2 in single cells. *Biophys. J.* 59:186–202.

Kowalczyk, A., N. Boens, V. Van den Bergh, and F. C. De Schryver. 1994. Determination of the ground-state dissociation constant by fluorimetric titration. *J. Phys. Chem.* 98:8585–8590.

Kuipers, O. P., M. Vincent, J. C. Brochon, H. M. Verheij, G. H. De Haas, and J. Gallay. 1991. Insight into the conformational dynamics of specific regions of porcine pancreatic phospholipase A_2 from a time-resolved fluorescence study of a genetically inserted single tryptophan residue. *Biochemistry.* 30:8771–8785.

Marks, P. W., and F. R. Maxfield. 1991. Preparation of solutions with free calcium concentration in the nanomolar range using 1,2-bis(o-aminophenoxy)ethane-N,N,N′,N′-tetraacetic acid. *Anal. Biochem.* 193:61–71.

Marquardt, D. W. 1963. An algorithm for least-squares estimation of nonlinear parameters. *J. Soc. Ind. Appl. Math.* 11:341–441.

Moore, E. D., P. L. Becker, K. E. Fogarty, D. A. Williams, and F. S. Fay. 1990. Ca^{2+} imaging in single living cells. *Cell Calcium.* 11:157–179.

O'Connor, D. V., and D. Phillips. 1984. Time-Correlated Single Photon Counting. Academic Press, London.

Smith, B. T., J. M. Boyle, B. S. Garbow, Y. Ikebe, V. C. Klema, and C. B. Moler. 1974. Lecture Notes in Computer Science, Vol. 6. G. Goos and J. Hartmanis, editors. Springer-Verlag, Berlin.

Tsien, R. Y. 1991. Fluorescent probes for cell signaling. *Annu. Rev. Neurosci.* 12:227–253.

Tsien, R. Y., T. Y. Rink, and M. Poenie. 1985. Measurement of cytosolic free Ca^{2+} in individual cells using fluorescence microscopy with dual excitation wavelengths. *Cell Calcium* 6:145–157.

Van den Bergh, V., N. Boens, F. C. De Schryver, M. Ameloot, J. Gallay, and A. Kowalczyk. 1992. One-step parameter estimation of the acid-base equilibria in the ground and excited states of 2-naphthol by global compartmental analysis of the fluorescence decay surface. *Chem. Phys.* 166:249–258.

Weller, A. 1961. Fast reactions of excited molecules. *Prog. React. Kinet.* 1:187–214.